crystals

MDPI

Article

Optical Investigation of Eu^{3+} Doped $Bi_{12}GeO_{20}$ (BGO) Crystals

M. Kowalczyk [1,*], T.F. Ramazanova [2], V.D. Grigoryeva [2], V.N. Shlegel [2], M. Kaczkan [1], B. Fetliński [1] and M. Malinowski [1]

[1] Institute of Microelectronics and Optoelectronics, Warsaw University of Technology, Koszykowa 75, 00-662 Warsaw, Poland

[2] Institute of Inorganic Chemistry, Siberian Branch, Russian Academy of Sciences, Novosibirsk 630090, Russia

* Correspondence: M.Kowalczyk.8@elka.pw.edu.pl; Tel.: +48-512-729-892

Received: 21 March 2020; Accepted: 7 April 2020; Published: 9 April 2020

Abstract: The spectroscopic properties of Eu^{3+} doped $Bi_{12}GeO_{20}$ (BGO) sillenite bulk crystals that were grown by the low-thermal-gradient Czochralski technique (LTG Cz) were investigated. The absorption spectra and the emission properties have been measured at room temperature (300 K) and at 10 K. Luminescence was observed both due to the direct Eu^{3+} ion excitation, as well as under UV excitation due to the energy transfer between Bi^{3+} and Eu^{3+} ions. $Bi^{3+} \rightarrow Eu^{3+}$ energy transfer mechanisms in Eu^{3+}:BGO doped host were investigated. The Ω_λ parameters, as well as radiative lifetimes, were calculated based upon the Judd-Ofelt formalism. The branching ratios and electric dipole transition probabilities were also determined, based upon the obtained experimental results. Luminescence has been observed from the $^5D_{0,1,2}$ levels of Eu^{3+}, with emissions from the $^5D_0$ level being the strongest. The strongest observed luminescence band corresponds to the $^5D_0 \rightarrow {}^7F_0$ transition at 578.7 nm. Reasons for the strong presence of the theoretically forbidden $^5D_0 \rightarrow {}^7F_0$ emission were investigated.

Keywords: Eu^{3+} luminescence; spectroscopy; $Bi_{12}GeO_{20}$; Bi^{3+} to Eu^{3+} transfer

1. Introduction

$Bi_{12}GeO_{20}$ (BGO) crystal finds application in many photonic devices and systems [1–6]. For example, it is commonly found in Pockels cells and sensors due to its high electro-optic coefficient (3.3 pm/V) [1,2]. It is also used in piezoelectric, Surface Acoustic Wave (SAW) devices [5]. The early works mainly focused on photorefractive and photoconductive effects in BGO and their applications within the visible light spectrum, such as early optical memory storage trials [6–8]. In recent years, metal-ion doping of BGO and other sillenites (mostly with 3d transition metal ions, such as Cr, Fe, Cu, Co, etc.) has been extensively studied as a means of further improving their efficiency as a holographic memory medium [9–14].

The pure $Bi_{12}GeO_{20}$ structure and properties have already been thoroughly investigated as early as in 1967 in its undoped form and many practical applications were proved [1–8]. BGO has a structure of the type of sillenite, which belongs to the space group I23 number 197 and possesses a cubic cell symmetry with lattice constant that is equal to 10.1455 Å and unit-cell volume of 1044.288244 $Å^3$, whereas the Bi-O bond lengths vary between 2.07 and 3.17 Å, as reported in the literature [1].

Generally, luminescence occurs when excitation radiation is absorbed by the material and electron transitions from the ground state ($^1S_0$ in case of Bi^{3+} and $^7F_0$ in case of Eu^{3+}) to one of the higher lying states, such as, for example, $^3P_1$ or $^3P_0$ states for Bi^{3+} ion and $^5D_0$, $^5D_1$, $^5D_2$, or $^5D_3$ states in the case of the Eu^{3+} ion. Upon return to the ground state from the excited state, a photon is emitted, resulting in observable luminescence of a given material. In special cases, such as in the case of the Eu^{3+} and Bi^{3+}

ions, positions of their respective energy levels are aligned, allowing for an efficient energy transfer between the ions, as has been illustrated on Figure 1.

The trivalent europium ion (Eu^{3+}) ion is uniquely suited in its role as a spectroscopic probe for the investigation of properties of various dielectric matrixes. This is because the $^5D_0$ and $^7F_0$ energy levels of Eu^{3+} are non-degenerate, resulting in a single line for transition between these levels in the spectra (see the partial Eu^{3+} energy diagram in Figure 1). Additionally, because the $^5D_0 \rightarrow {}^7F_1$ transition is of a magnetic dipole origin, its intensity is independent of the environment and, thus, can be applied as a reference to other transitions during emission spectrum analysis [15].

In this work, we have applied the Judd-Ofelt theory [15,16] to analyze and describe the BGO:Eu^{3+} crystal system photoluminescence and excited states dynamics, in order to further expand the knowledge regarding the Eu^{3+} interaction in a isotropic I23 class sillenite crystal system, and to evaluate its further potential uses, for example, as an active lasing medium candidate. The doubly reduced matrix elements $U^2_{2,4,6}$ elements have non-zero value for only single parameter U^2 for a given transition, which makes it possible to determine the intensity $\Omega_{2,4,6}$ parameters in a relatively straightforward manner just from emission spectra alone, which is not possible in the case of other lanthanide ions [15]. The $\Omega_{2,4,6}$ parameters allow for the determination of crucial factors, such as emission transition probabilities, which is important, for example, where considering a given material as a lasing medium candidate [15,16].

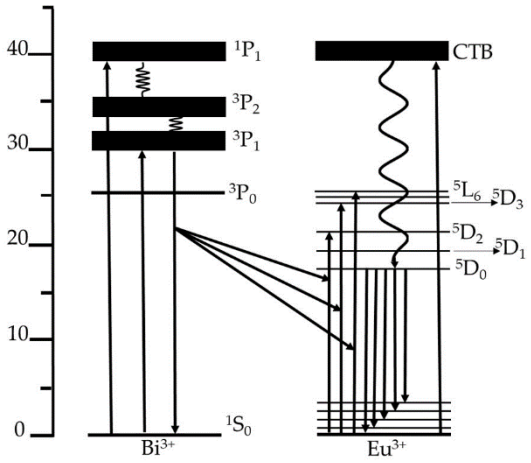

Figure 1. The partial energy diagram of Eu^{3+} and Bi^{3+} ions.

2. Materials and Methods

2.1. Crystal Growth

For crystal growth, the low-thermal-gradient Czochralski (LTG Cz) technique was used. The LTG Cz technique was developed at Nikolaev Institute of Inorganic Chemistry SB RAS (Novosibirsk, Russia) for growing large oxide crystals from melt. It is a modified Czochralski technique with axial and radial temperature gradients being sustained below 1 K/cm during the entire growth process, which is 1–2 orders of magnitude lower than in the conventional Czochralski technique. As a consequence, local overheating of the melt is eliminated, volatilization of melt components is suppressed, and the amount of thermoelastic stresses in the crystals is greatly lowered, which is extremely important for obtaining large single crystals of high optical quality. Using LTG Cz technique, numerous scintillating crystals of unique quality and size were obtained, such as $Bi_4Ge_3O_{12}$, $CdWO_4$, $ZnMoO_4$, and Li_2MoO_4 [17].

Previously, undoped $Bi_{12}GeO_{20}$ and $Bi_{12}SiO_{20}$ crystals were grown by LTG Cz at Nikolaev Institute of Inorganic Chemistry SB RAS (Novosibirsk, Russia) during the investigation of temperature gradients influence on crystal morphology and quality. Low temperature gradients conditions and the resulting faceted crystallization front proved to be more suitable for growing $Bi_{12}GeO_{20}$ (BGO) single crystals [18].

In this work, three Eu^{3+} doped BGO single crystals (0.3 mol.%, 1 mol.%, and 3 mol.%) were obtained by the low-thermal-gradient Czochralski technique. Crystal growth experiments were carried out in platinum crucible covered with platinum lid with a pipe socket at air atmosphere. Seeding in first crystal growth process was conducted on platinum seed holder, and a polycrystal was grown, from which seeds for further experiments were cut out. The BGO single crystals were grown in [001] direction with growth rate 1 mm/h and rotation rate 20 rpm. Crystals showed a strong tendency to the rapid development of square cross-section and lateral faceting. The crystallization fronts of grown crystals were faceted by single (001) facet.

The doping concentration was 0.3, 1, and 3 mol.%. From grown crystals (as shown in Figure 2), samples for optical studies were cut out, perpendicularly to [001] axis, and then polished: $20 \times 20 \times 10$ mm^3 samples from 0.3 and 1 mol.% doped crystals and $10 \times 10 \times 5$ mm^3 samples from 3 mol.% doped crystal. In accordance with the Goldschmidt substitution rules, the Eu^{3+} ion (1.07 Å) substitutes the Bi^{3+} (0.96 Å) atom within the Eu:BGO crystal cell. The difference between the radii of Ge^{4+} (0.39 Å) and Eu^{3+} is too large to allow for potential Ge^{4+} substitution. The pure BGO cell structure is shown in Appendix A for reference. The XRD technique confirmed the structure of the Eu^{3+}: BGO sample. All of the recorded diffraction peaks agree well with the standard card for the $Bi_{12}GeO_{20}$ and no additional peaks were observed, which suggested that the $Bi_{12}GeO_{20}$ crystals were successfully synthesized and the substitution of Eu^{3+} ions did not significantly change the crystal structure (as shown in Appendix A).

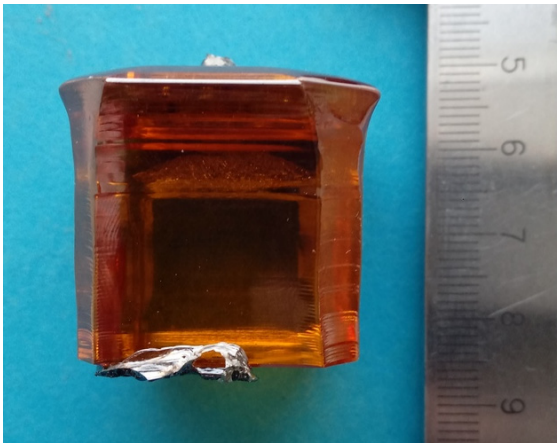

Figure 2. $Bi_{12}GeO_{20}$ (BGO) crystal doped with 0.3 mol.% Eu^{3+}.

2.2. Samples Characterization

The absorption spectrum was taken at room temperature using a Perkin–Elmer Lambda 950 spectrophotometer. Emission measurements were performed while using a Photon Technology International spectrophotometer. Emission spectra were also measured using a SP-2500i double set monochromator followed by a PMT and SR-400 photon counting system. The samples were excited by a pulsed (10 ns pulse-width, repetition rate 10 Hz) tunable optical parametric oscillator (Continuum) that was pumped by a frequency-tripled Nd: YAG pulse laser (Continuum Surelite II). The fluorescence dynamics profiles were recorded with a SR-430 multi-channel analyzer that was controlled with a PC computer. Sample cooling was provided by a closed cycle He optical cryostat, which allowed for the temperature to be varied between 10 and 300 K.

3. Results and Discussion

Absorption and emission spectra were recorded at room temperature (300 K) and at 10 K using the cryostat setup. The BGO crystal absorption spectrum taken in room temperature can be seen in Figure 3. A strong absorption edge can be seen in the UV-short wavelength VIS region. It is worthwhile to note that this absorption "shoulder" exists due to the incorrect occupation of Bi_{Ge} centers (notation

as used in [19]) within the crystal matrix, as indicated in literature [19]. The position of the $^5D_0 \leftarrow {}^7F_0$ level of Eu^{3+} has been determined from the low temperature absorption spectrum to be 17277 cm^{-1} (578.8 nm) in BGO. Only single maximum of the $^5D_0 \leftarrow {}^7F_0$ line has been observed, with line spectral width being equal to 0.09 nm, as seen in Figure 4.

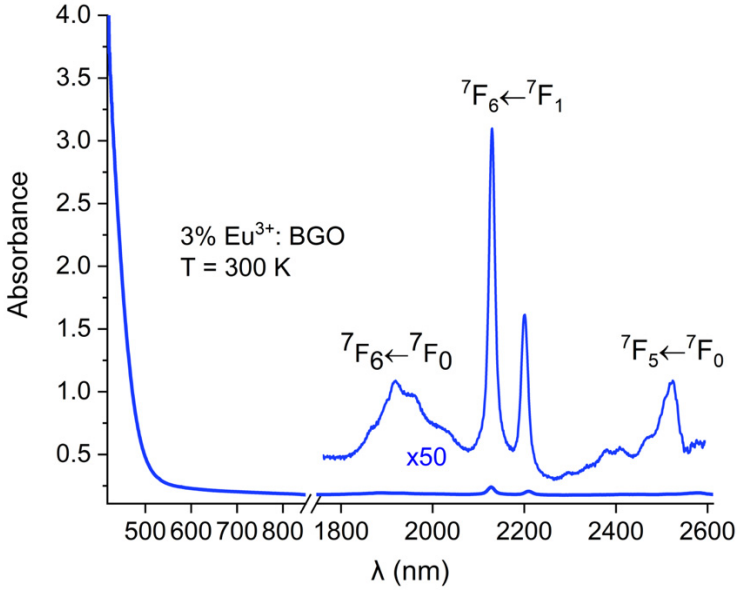

Figure 3. Absorption spectrum of BGO: 3% Eu^{3+} at T = 300 K.

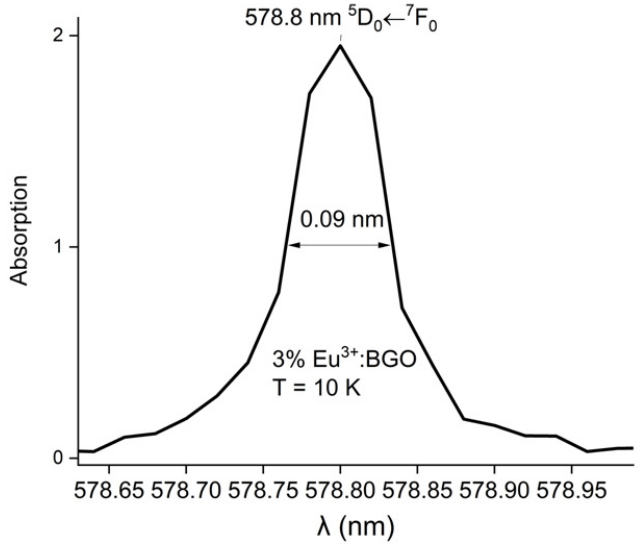

Figure 4. Low temperature (10 K) absorption spectrum where $^5D_0 \leftarrow {}^7F_0$ line is shown.

The emission spectra of the BGO samples were recorded at room temperature (300 K) and at 10 K. Emission spectrum of Eu^{3+} in BGO from the $^5D_0$ level can be seen in Figure 5, where all transitions except rarely observed $^5D_0 \rightarrow {}^7F_5$ and $^5D_0 \rightarrow {}^7F_6$ are shown. Eu^{3+} luminescence in BGO occurs due to direct excitation of Eu^{3+}, as well as via $Bi^{3+} \rightarrow Eu^{3+}$ energy transfer. In Figure 6 emission from higher lying states $^5D_1$ and $^5D_2$ can also be observed, although it is of much lower intensity when compared to the $^5D_0$ emissions.

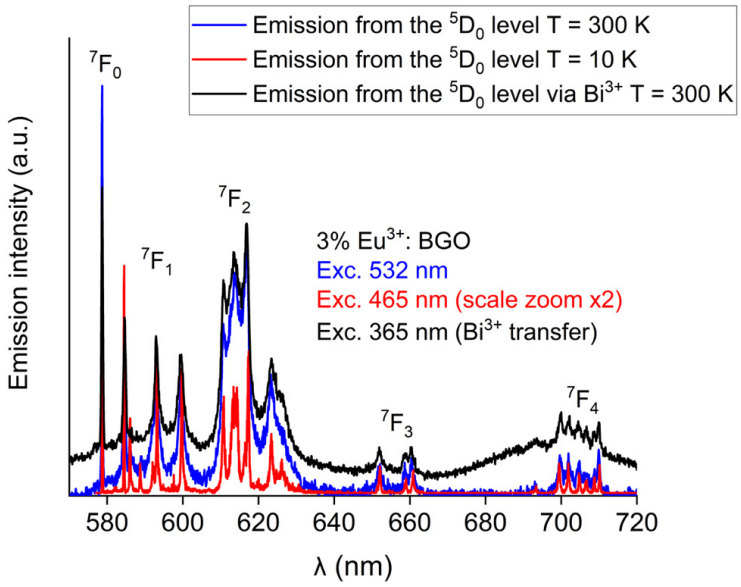

Figure 5. $^5D_0$ level emission spectra of BGO: 3% Eu^{3+}.

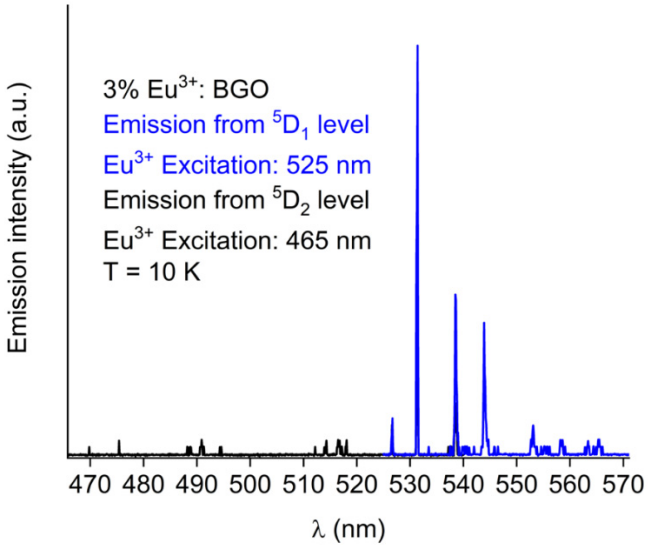

Figure 6. $^5D_2$ and $^5D_1$ levels emission spectra of BGO: 3% Eu^{3+}.

It is prudent to include the studies of interaction between the Bi^{3+} host ions and introduced Eu^{3+} dopant since the Bi^{3+} ion, which constitutes a core component of the BGO host lattice, is also optically active [20]. The Bi^{3+} within the host matrix, which is partially substituted by Eu^{3+} dopant, is heptacoordinated and possesses C_{1h} site symmetry, which is confirmed by means of analysis of the Europium emission spectra [21]. The emission of Bi^{3+} ion is a broad-band type emission, which is based upon transition from the ground state $^1S_0$ state to the $^3P_1$ or $^3P_0$ state (see Figure 1). Those transitions lay in the UV portion of the spectrum in which both pure as well as Eu^{3+}-doped BGO exhibits strong absorption. It has been reported by G. Blasse and A. Bril [22] that the positions of the Bi^{3+} $^1S_0 \rightarrow {}^3P_1$ band and the charge transfer (CT) band of Eu^{3+} permit the occurrence of successful energy transfer between Bi^{3+} and Eu^{3+} ions through UV excitation of Bi^{3+} [23]. Therefore, the Bi^{3+} ion can be utilized as an effective luminescence sensitizer for Eu^{3+} by means of non-radiative energy transfer, as further stipulated [22,23]. It is important to note that the efficiency of the transfer as well as excitation energy required for successful transfer strongly depend on the host matrix [20]. In order to evaluate the presence and efficiency of the Bi-Eu energy transfer in BGO Bi^{3+} excitation spectra were measured in all of the samples, including reference pure BGO sample. Bi^{3+} excitation band maximum

lies at 365 nm, which is in full agreement with studies that were performed on pure samples by G. Blasse and C.W.M. Timmermans, as seen in Figure 7 [21]. The study also mentions that Bi^{3+} excitation within the BGO matrix is also possible by 355 nm light. This has also been successfully verified during luminescence emission measurements, although 355 nm excitation results with emission of lower efficiency, as compared to 365 nm excitation in room temperature (300 K).

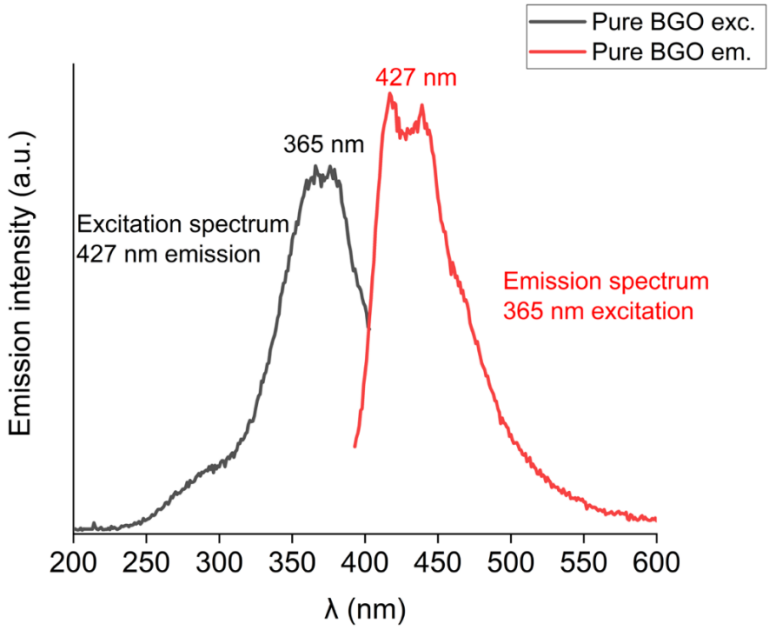

Figure 7. The Bi^{3+} ion excitation and emission spectrum in BGO (T = 300 K).

The emission profile of Eu:BGO can be seen in Figure 8, as expressed in CIE 1976 color space.

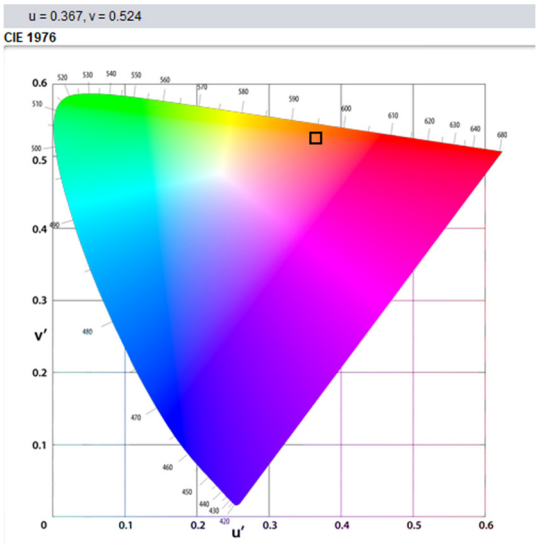

Figure 8. The emission profile of Eu:BGO as expressed in CIE 1976 color space.

The measured Bismuth radiative decay times shorten substantially with the increase of the Europium concentration, which proves the efficiency of the observed energy transfer in T = 300 K (as shown in Figure 9). Furthermore, radiative decay measurements of the $^5D_0$ level, when excited via $^5D_1$ or $^5D_2$ levels, show the clear presence of a rise time in the beginning, which indicates that luminescence from higher-lying $^5D_1$ and $^5D_2$ levels of Eu^{3+} is also additionally occurring (as shown in Figure 10). Additionally, the calculated theoretical radiative luminescence decay time is significantly longer than

observed, which can be attributed to the presence of strong $^5D_0 \rightarrow {}^7F_0$ line, the contribution of which is not taken into account by the classical Judd-Ofelt theory [16,24,25], as discussed further.

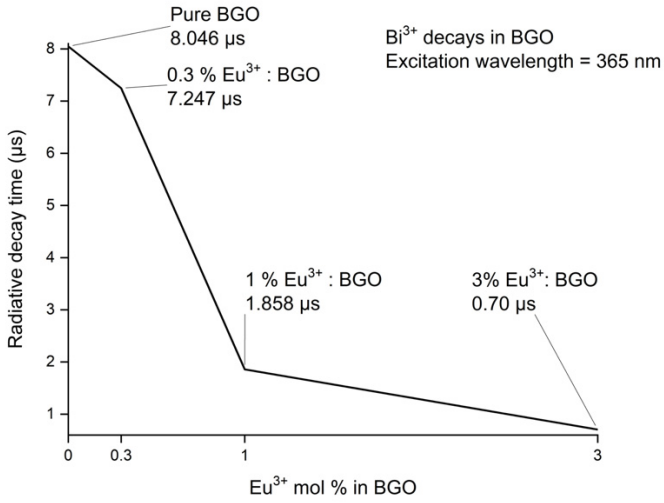

Figure 9. Bi^{3+} decay times relative to the Eu^{3+} concentration (measured at T = 300 K).

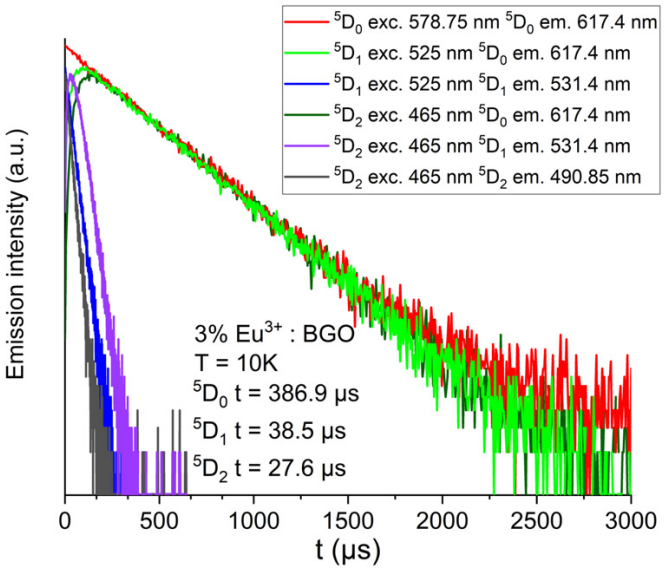

Figure 10. BGO: 3% Eu^{3+} excitation decays originating from different levels at T = 10 K.

The Judd-Ofelt (J–O) theory [16,24,25] is a well-recognized method for the analysis and comparison of the spectroscopic properties of rare-earth (RE^{3+}) ions in dielectric matrixes. For most RE^{3+} elements, calculation is solely based upon tabulated reduced matrix elements and integrated absorption cross section measurements. By applying the symbol convention that is based upon the formulas derived in [15], it is possible to describe dipole strength (expressed in Debye^2), based upon absorption spectra integrated peak areas, as:

$$D_{exp} = \frac{1}{108.9 * C * d * X_A(T)} * \int \frac{A(\tilde{v})}{\tilde{v}} d\tilde{v} \quad (1)$$

where $\tilde{v}$ is the mean wavenumber of the transition in cm^{-1}, C is the mol dopant concentration, d is the optical path length, and $X_A(T)$ is the fractional thermal population at temperature T of level A from which the absorption process begins. Furthermore, the calculated dipole strength can be computed while using the following equation:

$$D_{calc} = \frac{10^{36}}{2J+1} * X_{ED} * e^2 * \sum_{\lambda=2,4,6} \Omega_\lambda \left| \langle J \left\| U^{(\lambda)} \right\| J' \rangle \right|^2 \quad (2)$$

whereas 10^{36} is the D^2 into esu x cm conversion factor, e^2 is the elementary charge, $2J + 1$ denotes the degeneracy of the ground state, and $\left| \langle J \left\| U^{(\lambda)} \right\| J' \rangle \right|^2$ are the squared reduced matrix elements, which were tabulated and made available by the works of Carnall et al. [26], while the term $X_{ED} = \frac{(n^2+2)^2}{9n}$ accounts for the correction of the effect in the dielectric medium, and where n denotes its refractive index. As Judd-Ofelt calculations are often performed using the oscillator strength parameter, the dipole strength D and oscillator strength f can be converted using the following relation:

$$D = \frac{2.124 * 10^6 f}{\tilde{v}} \quad (3)$$

It is important to remark that the Eu^{3+} ion has a unique property of having reduced matrix elements that are mostly equal to zero, with the exception of only non-zero values $\|U^2\|^2$ for $^5D_0 \rightarrow {}^7F_2$ transition and for $\|U^4\|^2$ and$\|U^6\|^2$ elements for $^5D_0 \rightarrow {}^7F_4$, and $^5D_0 \rightarrow {}^7F_6$ transitions, respectively. Therefore, it is possible to derive the values of Judd-Ofelt Ω_λ parameters for Eu^{3+} - doped hosts, based on the integrated areas of the emission spectra alone. Since the $^5D_0 \rightarrow {}^7F_1$ magnetic-dipole transition is independent of the host environment, it can be used as a reference one for transitions with the $^5D_0$ excited state as origin. Based upon the work of K. Binnemans [15], the A_{ref} value for $^5D_0 \rightarrow {}^7F_1$ transition can be calculated using the formula:

$$\frac{1}{\tau_{rad}} = A_{MD,0} n^3 * \left(\frac{I_{tot}}{I_{MD}} \right) \quad (4)$$

where n is the refractive index of the host and $A_{MD,0}$ is the spontaneous emission probability for the $^5D_0 \rightarrow {}^7F_1$ magnetic dipole transition in vacuo, which is equal to 14.65 s^{-1} [15]. Therefore, it is possible to calculate the Ω_λ parameters from the ratio of the integrated intensity of the $^5D_0 \rightarrow {}^7F_{2,4,6}$ transitions (referenced as $\int I_\lambda(\tilde{v})d\tilde{v}$ in the following equation) to the ratio of the integrated intensity of the $^5D_0 \rightarrow {}^7F_1$ magnetic dipole transition (indicated as $\int I_1(\tilde{v})d\tilde{v}$ in the following equation) by applying the following equation [15]:

$$\Omega_\lambda = \frac{D_{MD}\tilde{v}_1^3}{e^2\tilde{v}_\lambda^3 \left| \langle \Psi J \left\| U^{(\lambda)} \right\| \Psi J' \rangle \right|^2} * \frac{9n^3}{n(n^2+2)^2} * \frac{\int I_\lambda(\tilde{v})d\tilde{v}}{\int I_1(\tilde{v})d\tilde{v}} \quad (5)$$

where $\tilde{v}_1$ is the averaged wavenumber of the $^5D_0 \rightarrow {}^7F_1$ transition and $\tilde{v}_\lambda$ is the averaged wavenumber of the $^5D_0 \rightarrow {}^7F_\lambda$ transition, where λ = 2,4,6. The averaged wavenumber can be calculated according to the formula:

$$\tilde{v}_\lambda = \frac{\int \tilde{v} I(\tilde{v})d\tilde{v}}{\int I(\tilde{v})d\tilde{v}} \quad (6)$$

As derived and discussed by K. Binnemans [15], since the $^5D_0 \rightarrow {}^7F_6$ transition is usually very rarely observed, it is often possible to calculate just the Ω_2 and Ω_4 parameters Given that for $^5D_0 \rightarrow {}^7F_1$ magnetic-dipole transition the dipole strength can be expressed as $D_{MD} = 9.6 \times 10^{-6}$ Debye^2, and assuming that for other transitions $D_{MD} = 0$, for transitions $^5D_0 \rightarrow {}^7F_{2,4,6}$ D_{ED} is equal to the following:

$$D_{ED} = e^2 \sum\nolimits_{\lambda=2,4,6} \Omega_\lambda \left| \langle \Psi J \left\| U^{(\lambda)} \right\| \Psi J' \rangle \right|^2 \quad (7)$$

Furthermore, for transitions $^5D_0 \rightarrow {}^7F_{0,3,5}$ both D_{ED} and D_{MD} are assumed to be equal to zero [15]. Taking into account all of the above, it is now possible to calculate the radiation transition probabilities of all excited states while using the Judd-Ofelt parameters using the formula [15]:

$$A(\Psi J, \Psi' J') = \frac{64\pi^4 \tilde{v}^3}{3h(2J+1)} * [\frac{n(n^2+2)^2}{9} * D_{ED} + n^3 D_{MD}] \quad (8)$$

where $\tilde{v}$ is the average wavenumber of the transition in cm^{-1}, h is equal to the Planck constant and $2J + 1$ denotes the degeneracy of the initial state. In addition, the radiative branching ratios $\beta_R(\Psi J, \Psi' J')$ from level J to J' can now be calculated while using the $A(\Psi J, \Psi' J')$ values from the equation above, as [15]:

$$\beta_R(\Psi J, \Psi' J') = \frac{A(\Psi J, \Psi' J')}{\sum_{\Psi' J'} A(\Psi J, \Psi' J')} \quad (9)$$

By applying the standard least-squares method, for which the root mean square (RMS) deviation can be defined, as follows:

$$RMS = \sqrt{\frac{\sum_i (D^i_{exp} - D^i_{calc})^2}{N-3}} \quad (10)$$

where N equals the number of transitions used in the fitting procedure and 3 is the number of fitted parameters $(\Omega_2, \Omega_4, \Omega_6)$, it is now possible to iteratively fit the Ω_λ parameters.

Furthermore, the asymmetry parameter (calculated from the room temperature emission spectrum) R is defined as the ratio between the integral intensities of the $^5D_0 \rightarrow {}^7F_2$ and $^5D_0 \rightarrow {}^7F_1$ transition bands, $R = I(^5D_0 \rightarrow {}^7F_2)/I(^5D_0 \rightarrow {}^7F_1)$ may be considered as an indication of the Eu^{3+} ion symmetry. Specifically, the further from a centrosymmetric geometry luminescent center is located, the higher the value of the asymmetry parameter R [15,27]. As expected, the determined R parameter for Eu^{3+}:BGO specimens increases for samples with higher concentration of Europium^{3+}, as the Eu^{3+} ion somewhat disrupts lattice symmetry, which is due to the difference between the ionic radii of Bi^{3+} (0.96 Å) and Eu^{3+} (1.07 Å) ions, as indicated in Table 1.

Table 1. Comparison of asymmetry ratios in relation to doping concentration in different Eu^{3+}:BGO samples.

Eu^{3+} Concentration (mol %)	R Value
3	2.493
1	2.347
0.3	1.820

Eu^{3+}:BGO emission spectra were recorded at T = 300 K and 10 K, Judd-Ofelt parameters, asymmetric and branching ratios were calculated. Table 2 shows the spontaneous emission probabilities, fluorescence branching ratios and radiative lifetimes of Eu^{3+}:BGO using the calculated parameters. The obtained theoretical radiative lifetime is significantly longer than the experimentally observed value, which indicates that all of the occurring processes are not taken into account by the Judd-Ofelt theory (such as the very strong presence of the $^5D_0 \rightarrow {}^7F_0$ emission line). Comparison of Judd-Ofelt parameters between Eu^{3+}:BGO and other Eu^{3+}-doped hosts is shown in Table 3. The Judd-Ofelt parameter Ω_2 can be generally used to represent the strength of the covalency and the site symmetry of Eu^{3+}, as mentioned above [15,27,28]. The value of Ω_2 in Eu:BGO is larger than the values reported for Eu^{3+}:LaF_3 and Eu^{3+}:$YAlO_3$ materials, and smaller than the values reported for the other listed materials. Similar observations have been reported in [28] for the Eu^{3+} doped scintillating crystal $Bi_4Ge_3O_{12}$, also possessing cubic symmetry (although it has a different space group (43d) than Eu:BGO). This trend confirms that the values of, and relations between, the derived Ω_λ parameters, are strongly host-dependent, and thus can be used as a general indicator of the host symmetry.

Table 2. The spontaneous emission probabilities, fluorescence branching ratios and asymmetry ratio of BGO: 3% Eu^{3+} calculated using the obtained Judd-Ofelt parameters.

Transition	λ (nm)	$A_{calc}(s^{-1})$	β_{calc}
$^5D_0 \rightarrow {}^7F_0$	578	0	0
$^5D_0 \rightarrow 7F_1$	584	249.258	0.2557
$^5D_0 \rightarrow 7F_2$	614	652.459	0.6694
$^5D_0 \rightarrow {}^7F_3$	660	0	0
$^5D_0 \rightarrow {}^7F_4$	705	72.955	0.0748
$^5D_0 \rightarrow {}^7F_5$	-	-	-
$^5D_0 \rightarrow {}^7F_6$	-	-	-
Σ		974.672	1
$\Omega_2 = 3.12224 \times 10^{-20}$ cm^2			
$\Omega_4 = 0.77412 \times 10^{-20}$ cm^2			
$\tau_{calc} = 1025.9$ μs			

Table 3. The comparison of Judd-Ofelt parameters in different Europium doped hosts.

Compound	Ω_2 (10^{-20} cm^2)	Ω_4 (10^{-20} cm^2)	Ω_6 (10^{-20} cm^2)	Reference
$Bi_{12}GeO_{20}$	3.12	0.77	-	This work
$Bi_4Ge_3O_{12}$	4.39	2.70	0.64	[28]
$KLu(WO_4)_2$	20.76	5.23	7.96	[29]
$KY(WO_4)_2$	36.70	11.50	3.40	[30]
$NaY(WO_4)_2$	8.61	1.12	0.47	[31]
$Y_4Al_2O_9$	5.65	2.62	2.63	[32]
LaF_3	1.19	1.16	0.39	[33]
$YAlO_3$	2.66	6.33	0.80	[33]
ZnO	9.59	8.11	0.25	[33]
Y_2O_3	9.86	2.23	0.32	[33]
Gd_2O_3	12.39	2.02	0.19	[34]

The presence of a strong $^5D_0 \rightarrow {}^7F_0$ emission line, as observed in the emission spectra (shown in Figure 5), should not be disregarded (even though this ED transition is considered "forbidden" by classical Judd-Ofelt theory [24,25]), since the standard model effectively does not take into account the J–J mixing and the spin–orbit interaction [35]. In fact, the presence of a strong $^5D_0 \rightarrow {}^7F_0$ emission line can be attributed to the vibronic coupling or via mixing of higher configurations into the 4f wavefunctions by the crystal-field effect, as noted by K.Binnemans, [15]. Indeed, there are numerous cases shown of Eu^{3+} doped hosts with low local site symmetries (C_s, C_n, C_{nv}), in which the $^5D_0 \rightarrow {}^7F_0$ emission is very strong or even strongest of the entire spectrum [35] (as a notable example, the $^5D_0 \rightarrow {}^7F_0$ emission line of strong intensity has also been observed in Eu^{3+}: $Bi_4Ge_3O_{12}$, as reported in [36]). Furthermore, the ratio of the integrated intensity of the $^5D_0 \rightarrow {}^7F_0$ / $^5D_0 \rightarrow {}^7F_1$ transitions is an important factor that represents the contribution due to the J − J mixing and the spin–orbit interaction, as noted in [35,37]. It can be expressed formally as $R_{JJ} = I(^5D_0 \rightarrow {}^7F_0)/I(^5D_0 \rightarrow {}^7F_1)$ and in case of 3% Eu:BGO equals 0.2962. Additionally, it is important to mention that, in some cases, the J–J mixing alone is insufficient to explain the intensity of the observed $^5D_0 \rightarrow {}^7F_0$ emission [35,37,38]. The Wybourne–Downer mechanism [39] and breakdown of the closure approximation in the Judd-Ofelt theory must then also be taken into account [40]. Additionally, the presence of only one narrow line for the $^5D_0 \rightarrow {}^7F_0$ transition of Eu^{3+} ion indicates that there is only one coordination environment of the Eu^{3+} ion, which is consistent with the structural data.

4. Conclusions

The spectroscopic properties of Eu^{3+} doped $Bi_{12}GeO_{20}$ (BGO) sillenite bulk crystals that were grown by the low-thermal-gradient Czochralski technique (LTG Cz) were investigated. The absorption spectra and the emission properties have been measured at room temperature (300 K) and at 10 K.

Based upon the absorption measurements at 10 K, position of the $^5D_0 \leftarrow {}^7F_0$ level of Eu^{3+} has been determined to be 17277 cm^{-1}. Luminescence has been observed from the $^5D_{0,1,2}$ levels of Eu^{3+}, with emissions from the $^5D_0$ level being the strongest one. Luminescence from the $^5D_0$ level was observed both due to the direct Eu^{3+} ion excitation, as well as under UV excitation due to the energy transfer between Bi^{3+} and Eu^{3+} ions (see Figure 5). Luminescence from the higher-lying $^5D_1$ and $^5D_2$ levels of Eu^{3+} has also been confirmed by means of radiative decay measurements (see Figure 10). The $Bi^{3+} \rightarrow Eu^{3+}$ energy transfer mechanisms were investigated. The Ω_λ parameters as well as radiative lifetimes were calculated based upon the Judd-Ofelt formalism. Branching ratios and electric dipole transition probabilities were also determined, based upon the obtained experimental results. The obtained values of the Ω_λ parameters are equal to $\Omega_2 = 3.12224 \times 10^{-20}$ cm^2 and $\Omega_4 = 0.77412 \times 10^{-20}$ cm^2, respectively. (see Table 2). Comparison between Eu:BGO and other Eu^{3+} doped hosts has been made (see Table 3). Reasons for the strong presence of the theoretically forbidden $^5D_0 \rightarrow {}^7F_0$ emission were also investigated and discussed.

The obtained results prove that the Eu:BGO crystals can be successfully utilized as a luminescent medium in the orange-red portion of the VIS region (see Figure 8). It is further worth noting that the excitation wavelengths for Eu:BGO are easily directly generated. This makes Eu:BGO an attractive alternative to similarly emitting materials, for which the generation of excitation wavelengths is difficult, thus making Eu:BGO a viable potential VIS laser material (in particular, the 532 nm and 355 nm excitation wavelengths are, respectively, the 2nd and 3rd harmonics of a widely available 1064 nm Nd:YAG laser, with sources of 365 nm wavelength also being widely available).

Author Contributions: Conceptualization, M.K. (M. Kowalczyk) and M.M.; Methodology, M.K. (M. Kowalczyk) and M.M.; Validation, M.K. (M. Kowalczyk), M.K. (M. Kaczkan), B.F. and M.M.; Investigation, M.K. (M. Kowalczyk), M.K. (M. Kaczkan) and B.F.; Resources, V.D.G., T.F.R. and V.N.S.; Writing—original draft preparation, M.K. (M. Kowalczyk); Writing—review and editing, M.K. (M. Kowalczyk), M.M. and V.D.G.; All authors have read and agreed to the published version of the manuscript.

Funding: This work was supported by the PROM project-International scholarship exchange of PhD candidates and academic staff (funded by NAWA – Polish National Agency for Academic Exchange).

Conflicts of Interest: The authors declare that they have no known competing financial interests.

Appendix A

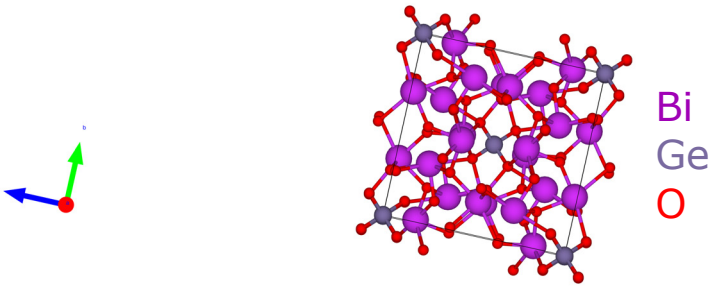

Figure A1. Crystal cell structure of BGO.

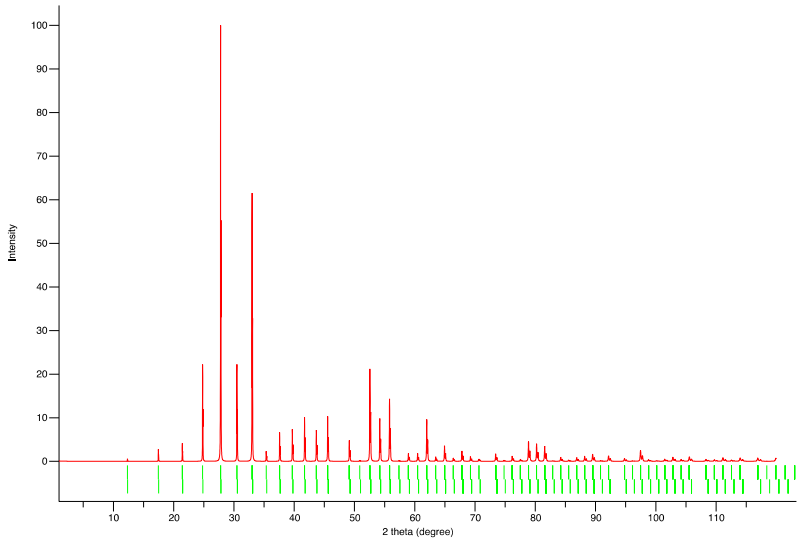

Figure A2. XRD spectrum of BGO.

References

1. Malinovskiy, V.K.; Gudaev, O.A.; Gusev, V.A.; Demenko, S.I. *Photoinduced Phenomena in Sillenite Crystals*; Nauka: Novosibirsk, Russia, 1990.
2. Abrahams, S.C.; Jamieson, P.B.; Bernstein, J.L. Crystal Structure of Piezoelectric Bismuth Germanium Oxide $Bi_{12}GeO_{20}$. *Chem. Phys.* **1967**, *44*, 4034–4041. [CrossRef]
3. Petricevic, S.J.; Mihailovic, P.; Radunovic, J. A miniature pockels cell with novel electrode geometry. *Sensors* **2009**, *9*, 5298–5307. [CrossRef] [PubMed]
4. Bridoux, E.; Rouvaen, J.M.; Coussot, C.; Dieulesaint, E. Rayleigh-Wave Propagation on $Bi_{12}GeO_{20}$. *Appl. Phys. Lett.* **1971**, *19*, 523–524. [CrossRef]
5. Wang, W.C.; Meng, K.S. Surface-wave correlation and time scaling in a structure of $Bi_{12}GeO_{20}$-Si-$LiNbO_3$. *Appl. Phys. Lett.* **1975**, *27*, 375–377. [CrossRef]
6. Huignard, J.P.; Micheron, F. High-sensitivity read-write volume holographic storage in BSO and BGO crystals. *Appl. Phys. Lett.* **1976**, *29*, 591–593. [CrossRef]
7. Peltier, M.; Micheron, F. Volume hologram recording and charge transfer process in $Bi_{12}SiO_{20}$ and $Bi_{12}GeO_{20}$. *J. Appl. Phys.* **1977**, *48*, 3683–3690. [CrossRef]
8. Douglas, G.G.; Zitter, R.N. Transport Processes of Photoinduced Carriers in Bismuth Germanium Oxide ($Bi_{12}GeO_{20}$). *J. Appl. Phys.* **1968**, *39*, 2133–2135. [CrossRef]
9. Briat, B.; Borowiec, M.T.; Rjeily, H.B.; Ramaz, F.; Hamri, A.; Szymczak, H. Combined optical/mcd/odmr investigations of photochromism in doubly-doped Bi_{12} GeO_{20}. *Radiat. Eff. Defects Solids* **2002**, *157*, 989–993. [CrossRef]
10. Wood, A.W.; Hunt, C.A.; Martin, J.J. The low-temperature photochromic and photorefractive response of bismuth germanium oxide doped with molybdenum. *J. Appl. Phys.* **2007**, *101*, 1–7. [CrossRef]
11. Stepanova, I.V.; Gorashchenko, N.G.; Subbotin, K.A.; Smirnov, V.A. Determination of the charge state of chromium in Cr:$Bi_{12}GeO_{20}$ single crystals by spectral luminescence methods. *Opt. Spectrosc. English Transl. Opt. i Spektrosk.* **2009**, *107*, 335–338. [CrossRef]
12. Lu, J.; Dai, Y.; Zhu, Y.; Huang, B. Density functional characterization of pure and alkaline earth metal-doped $Bi_{12}GeO_{20}$, $Bi_{12}SiO_{20}$, and $Bi_{12}TiO_{20}$ photocatalysts. *ChemCatChem* **2011**, *3*, 378–385. [CrossRef]
13. Marinova, V.; Lin, S.H.; Hsu, K.Y. Photorefractive Properties Enhancement of Doped Bismuth Sillenite Crystals. *Opt. Mem. Neural Netw. Inf. Opt.* **2011**, *20*, 7–22. [CrossRef]
14. Marinova, V.; Liu, R.C.; Lin, S.H.; Hsu, K.Y. Real-time holography in ruthenium-doped bismuth sillenite crystals at 1064 nm. *Opt. Lett.* **2011**, *36*, 1981–1983. [CrossRef]
15. Binnemans, K. Interpretation of europium(III) spectra. *Coord. Chem. Rev.* **2015**, *295*, 1–45. [CrossRef]

16. Hehlen, M.P.; Brik, M.G.; Krämer, K.W. 50th anniversary of the Judd-Ofelt theory: An experimentalist's view of the formalism and its application. *J. Lumin.* **2013**, *136*, 221–239. [CrossRef]
17. Shlegel, V.N.; Borovlev, Y.A.; Grigoriev, D.N.; Grigorieva, V.D.; Danevich, F.A.; Ivannikova, N.V.; Postupaeva, A.G.; Vasiliev, Y.V. Recent progress in oxide scintillation crystals development by low-thermal gradient Czochralski technique for particle physics experiments. *J. Instrum.* **2017**, *12*. [CrossRef]
18. Shlegel, V.N.; Pantsurkin, D.S. Growth of $Bi_{12}GeO_{20}$ and $Bi_{12}SiO_{20}$ crystals by the low-thermal gradient Czochralski technique. *Crystallogr. Rep.* **2011**, *56*, 339–344. [CrossRef]
19. Oberschmid, R. Absorption Centers of $Bi_{12}GeO_{20}$ and $Bi_{12}SiO_{20}$ Crystals. *Phys. Status Solidi* **1985**, *89*, 263–270. [CrossRef]
20. Boutinaud, P. Revisiting the spectroscopy of the Bi^{3+} ion in oxide compounds. *Inorg. Chem.* **2013**, *52*, 6028–6038. [CrossRef]
21. Timmermans, C.W.M.; Blasse, G. The Luminescence of Some Oxidic Bismuth and Lead Compounds. *J. Solid State Chem.* **1984**, *52*, 222–232. [CrossRef]
22. Blasse, G.; Bril, A. Study of energy transfer from Sb^{3+}, Bi^{3+}, Ce^{3+} to Sm^{3+}, Eu^{3+}, Tb^{3+}, Dy^{3+}. *J. Chem. Phys.* **1967**, *47*, 1920–1926. [CrossRef]
23. Blasse, G. The ultraviolet absorption bands of Bi^{3+} and Eu^{3+} in oxides. *J. Solid State Chem.* **1972**, *4*, 52–54. [CrossRef]
24. Ofelt, G.S. Intensities of Crystal Spectra of Rare-Earth Ions. *J. Chem. Phys.* **1962**, *37*, 511–520. [CrossRef]
25. Judd, B.R. Optical absorption intensities of rare-earth ions. *Phys. Rev.* **1962**, *127*, 750–761. [CrossRef]
26. Carnall, W.T.; Crosswhite, H.; Crosswhite, H.M. Energy level structure and transition probabilities in the spectra of the trivalent lanthanides in LaF_3. *Energy* **1978**.
27. Kolesnikov, I.E.; Povolotskiy, A.V.; Mamonova, D.V.; Kolesnikov, E.Y.; Kurochkin, A.V.; Lähderanta, E.; Mikhailov, M.D. Asymmetry ratio as a parameter of Eu^{3+} local environment in phosphors. *J. Rare Earths* **2018**, *36*, 474–481. [CrossRef]
28. Li, N.; Xue, Y.; Wang, D.; Liu, B.; Guo, C.; Song, Q.; Xu, X.; Liu, J.; Li, D.; Xu, J.; et al. Spectroscopic properties of Eu:$Bi_4Ge_3O_{12}$ single crystal grown by the micro-pulling-down method. *J. Lumin.* **2019**, *208*, 208–212. [CrossRef]
29. Loiko, P.A.; Dashkevich, V.I.; Bagaev, S.N.; Orlovich, V.A.; Mateos, X.; Serres, J.M.; Vilejshikova, E.V.; Yasukevich, A.S.; Yumashev, K.V.; Kuleshov, N.V.; et al. Judd-Ofelt analysis of spectroscopic properties of Eu^{3+}:$KLu(WO_4)_2$ crystal. *J. Lumin.* **2015**, *168*, 102–108. [CrossRef]
30. Loiko, P.A.; Dashkevich, V.I.; Bagaev, S.N.; Orlovich, V.A.; Yasukevich, A.S.; Yumashev, K.V.; Kuleshov, N.V.; Dunina, E.B.; Kornienko, A.A.; Vatnik, S.M.; et al. Spectroscopic and photoluminescence characterization of Eu^{3+}-doped monoclinic $KY(WO_4)_2$ crystal. *J. Lumin.* **2014**, *153*, 221–226. [CrossRef]
31. Tian, Y.; Chen, B.; Hua, R.; Yu, N.; Liu, B.; Sun, J.; Cheng, L.; Zhong, H.; Li, X.; Zhang, J.; et al. Self-assembled 3D flower-shaped $NaY(WO_4)_2$:Eu^{3+} microarchitectures: Microwave-assisted hydrothermal synthesis, growth mechanism and luminescent properties. *CrystEngComm* **2012**, *14*, 1760–1769. [CrossRef]
32. Kaczkan, M.; Turczyński, S.; Malinowski, M. Spectroscopic properties and Judd-Ofelt analysis of Eu^{3+} in $Y_4Al_2O_9$ crystals. *J. Lumin.* **2018**, *196*, 111–115. [CrossRef]
33. Liu, Y.; Luo, W.; Li, R.; Liu, G.; Antonio, M.R.; Chen, X. Optical spectroscopy of Eu^{3+} doped ZnO nanocrystals. *J. Phys. Chem. C* **2008**, *112*, 686–694. [CrossRef]
34. Liu, L.; Chen, X. Energy levels, fluorescence lifetime and Judd-Ofelt parameters of Eu^{3+} in Gd_2O_3 nanocrystals. *Nanotechnology* **2007**, *18*, 255704. [CrossRef]
35. Chen, X.Y.; Liu, G.K. The standard and anomalous crystal-field spectra of Eu^{3+}. *J. Solid State Chem.* **2005**, *178*, 419–428. [CrossRef]
36. Chu, Y.; Zhang, Q.; Li, Y.; Liu, Z.; Xu, J.; Zeng, H.; Wang, H. Hydrothermal synthesis of $Bi_4Ge_3O_{12}$: Eu^{3+} phosphors with high thermal stability and enhanced photoluminescence property. *J. Alloys Compd.* **2017**, *693*, 308–314. [CrossRef]
37. Smentek, L.; Kędziorski, A. F $\longleftrightarrow$ f electric dipole transitions; old problems in a new light. *J. Alloys Compd.* **2009**, *488*, 586–590. [CrossRef]
38. Souza, A.S.; Oliveira, Y.A.R.; Couto dos Santos, M.A. Enhanced approach to the Eu^{3+} ion $^5D_0 \rightarrow {}^7F_0$ transition intensity. *Opt. Mater. (Amst.)* **2013**, *35*, 1633–1635. [CrossRef]

39. Burdick, G.W.; Downer, M.C.; Sardar, D.K. A new contribution to spin-forbidden rare earth optical transition intensities: Analysis of all trivalent lanthanides. *J. Chem. Phys.* **1989**, *91*, 1511–1520. [CrossRef]
40. Tanaka, M.; Nishimura, G.; Kushida, T. Contribution of J mixing to the $^5D_0 - {}^7F_0$ transition of Eu^{3+} ions in several host matrices. *Phys. Rev. B* **1994**, *49*, 16917–16925. [CrossRef]